

THE ANISOTROPIC COMMON REFLECTION SURFACE OPERATOR

C. Vanelle, I. Abakumov, and D. Gajewski

email: *claudia.vanelle@uni-hamburg.de*

keywords: *CRS, Anisotropy, 3D, Finite Offset*

ABSTRACT

Multiparameter methods have developed into standard tools in seismic data processing. However, most operators are restricted to application to isotropic media. Whereas application of an isotropic operator will still lead to satisfactory stack results, further processing steps that interpret and evaluate isotropic stacking parameters will lead to erroneous results if anisotropy is present but not accounted for. In this paper, we derive relationships between the stacking parameters and anisotropic wavefield attributes that allow us to apply the common-reflection-surface (CRS) type operator to 3D media with arbitrary anisotropy for the zero-offset and finite-offset configurations. The operator itself is still parameterised purely in terms of wavefield attributes that are measured in the acquisition surface, i.e., no model assumptions are made. Numerical results confirm that the accuracy of the new operator is of the same order as that of its isotropic counterpart.

INTRODUCTION

Stacking methods have been applied in seismic data processing for more than 50 years for several reasons. First, stacking results in a simulated zero-offset section, i.e., a section where source and receiver coordinates coincide. Such a stacked section displays an enhanced signal-to-noise ratio compared to the original data. Furthermore, additional information is obtained in terms of stacking parameters.

In the classic common midpoint (CMP) method, stacking is carried out over offsets (Mayne, 1962). The stacking parameter, assumed to coincide with the normal moveout (NMO) velocity, is determined by semblance analysis (Taner and Koehler, 1969). Since the CMP concept was introduced several extensions have been suggested to stack not only over offsets but also over midpoints. Carrying out a stack in both midpoint and offset directions increases the number of traces and thus enhances the signal-to-noise ratio even further. Also, the stacking surface is described by additional parameters or wavefield attributes and therefore yields even more information.

The most prominent examples for these multiparameter stacking operators are the common reflection surface (CRS) method (Müller, 1999), multifocusing (Gelchinsky et al., 1999), and more recently non-hyperbolic CRS (Fomel and Kazinnik, 2013) and implicit CRS (Schwarz et al., 2014). Whereas the individual operators use slightly different parameterisations, they all have in common that the parameters have a physical interpretation in terms of wavefront curvatures and angles.

The parameters can be used for a variety of applications such as attribute-based time migration (Spinner, 2007), multiple suppression (Dümmong and Gajewski, 2008), prestack data enhancement and regularisation (Baykulov and Gajewski, 2009), NIP-wave tomography (Duvencek, 2004), diffraction imaging (Dell and Gajewski, 2011), and diffraction tomography (Bauer et al., 2016), to name but a few.

The interpretation of the stacking parameters in terms of wavefield attributes in the afore-mentioned operators is so far only valid in isotropic media. Therefore, attempts have been made to derive multiparameter expressions that consider anisotropy. Vanelle et al. (2012) have extended the implicit operator to account for anisotropy. Since it is a 2D formulation, their approach is restricted to a symmetry plane, but

it allows otherwise for arbitrary anisotropy. In addition to the angles and wavefront curvatures used in the isotropic variant, velocity derivatives occur in the anisotropic case, which means that model assumptions must be made in order to apply this operator. The anisotropic CRS approximation suggested by Xu and Stovas (2015) also depends on model assumptions.

In this manuscript, we derive relationships between the stacking parameters and the anisotropic wavefield attributes from geometrical considerations by following an approach similar to that by Shah (1973) and Hubral and Krey (1980). The parameters that describe the stacking surface are, as in the isotropic case, wavefront curvatures and angles measured in the registration surface. Since no assumptions on the model enter the derivation, it can be considered as an entirely data-driven approach.

We will show that the anisotropic CRS operator in two dimensions can be expressed in terms of four independent attributes. The shape of the operator, however, is the same as its isotropic counterpart, which allows only the determination of three parameters. In the anisotropic case, these three parameters are combinations of the anisotropic attributes. This means that for the stacking neglecting the presence of anisotropy will not compromise the result.

This changes as soon as the stacking parameters enter data processing for tasks that involve not only the computation of traveltimes but other application of the wavefront attributes. Since the physical interpretation of the parameters is different in the presence of anisotropy, application of the parameters under the assumption of isotropy can lead to false results. For example, applications based on ray tracing that use the incidence or emergence angle to the registration surface need to distinguish between ray (group) and phase angle. Ignoring this difference, e.g., for performing NIP-wave tomography (Duveneck, 2004) or diffraction tomography (Bauer et al., 2016), would lead to an erroneous velocity model. During this step, model assumptions are made, however, the determination of the stacking parameters remains entirely model independent.

Since in many cases it is assumed that the topmost layer under the registration surface is isotropic, the new anisotropic CRS operator may not appear to have immediate practical relevance. It is, however, an important step to enhance our understanding of the physics of the wavefield attributes that are nowadays an integral and established part of seismic data processing.

In this paper, we begin with the derivation of the anisotropic CRS operator for the zero-offset situation for monotypic waves in 2D. The derivation follows the same approach that Shah (1973) and Hubral and Krey (1980) have applied in the isotropic case. In the second part of the method section, we extend the operator to the general finite-offset case that is also pertinent for converted waves. The third part considers the 3D case for arbitrary anisotropy and wave type. We then demonstrate the accuracy of the new operator with simple numerical examples where an analytic solution for the wavefield parameters is available. The following discussion and conclusions bring our work to a close.

METHOD

The Common Reflection Surface (CRS) operator was introduced by Müller (1999). It describes a hyperbolic traveltime surface in midpoint and half-offset coordinates that is parameterised in terms of kinematic wavefield properties, namely angles and wavefront curvatures, under the assumption of isotropy. In this section, we derive a corresponding anisotropic operator. Our derivation follows the geometrical approach by Shah (1973) and Hubral and Krey (1980), however, we take into account that the medium under consideration may be anisotropic. This will lead us to a new CRS operator for monotypic waves in the zero-offset situation, beginning with the 2D case. In a second step, we introduce a corresponding finite-offset CRS operator by extending the results derived for the zero-offset case in conjunction with a traveltime expression introduced by Vanelle and Gajewski (2002). The resulting finite-offset operator is applicable to converted waves as well. In the third step, we generalise our results by means of ray theoretical considerations following Červený (2001) and Schleicher et al. (2001) to obtain a 3D finite-offset operator for arbitrary anisotropy and wave type.

Anisotropic CRS for 2D zero offset

Assuming that the traveltime is a 'good' function, it can be expanded into a Taylor series. We carry out the expansion in midpoint (x_m) and half-offset (h) coordinates until second order for an expansion point at

$x_m = x_0$ and $h = 0$, i.e., for zero offset,

$$t = t_0 + \frac{\partial t}{\partial x_m} \Delta x_m + \frac{\partial t}{\partial h} h + \frac{1}{2} \frac{\partial^2 t}{\partial x_m^2} \Delta x_m^2 + \frac{1}{2} \frac{\partial^2 t}{\partial h^2} h^2 + \frac{\partial^2 t}{\partial x_m \partial h} \Delta x_m h \quad , \quad (1)$$

where $\Delta x_m = x_m - x_0$. Restricting the derivation (for now) to monotypic waves and keeping reciprocity in mind, the following derivatives must vanish due to the symmetry with regards to interchanging the source and receiver position:

$$\frac{\partial t}{\partial h} = 0 \quad \text{and} \quad \frac{\partial^2 t}{\partial x_m \partial h} = 0 \quad . \quad (2)$$

In conclusion, the traveltine expression reduces to

$$t = t_0 + \frac{\partial t}{\partial x_m} \Delta x_m + \frac{1}{2} \frac{\partial^2 t}{\partial x_m^2} \Delta x_m^2 + \frac{1}{2} \frac{\partial^2 t}{\partial h^2} h^2 \quad . \quad (3)$$

This is a parabolic expression. It is, however, known that reflection traveltimes are better approximated by hyperbolic than parabolic operators (e.g., Ursin, 1982; Gjøystdal et al., 1984). To obtain a hyperbolic expression like the original isotropic CRS operator, we square Equation 3 and omit terms of order higher than two, which leads to

$$t^2 = \left(t_0 + \frac{\partial t}{\partial x_m} \Delta x_m \right)^2 + t_0 \frac{\partial^2 t}{\partial x_m^2} \Delta x_m^2 + t_0 \frac{\partial^2 t}{\partial h^2} h^2 \quad . \quad (4)$$

Our aim is now to express the remaining derivatives in terms of physically-intuitive wavefield attributes like in Müller's (1999) result for the isotropic case.

In the following, ray velocities are denoted by v , phase velocities by V , and slowness vectors by \mathbf{p} . A subscript 0 denotes a quantity taken at the expansion point, x_0 , and subscript m indicates a quantity taken at a position x_m . Note that v_0 and V_0 are not vertical velocities but velocities taken in the expansion point x_0 associated with the ray and slowness direction at x_0 , respectively. Furthermore, angles ϑ are ray (group) angles and Θ are phase angles. Angles $\psi = \vartheta - \Theta$ lie between phase and ray direction.

Figure 1a displays a sketch of two zero-offset rays and their associated wavefronts arriving at locations x_m and x_0 in the registration surface. In addition to the ray angles ϑ_m and ϑ_0 , the figure shows the radius of curvature of the incident wavefront at x_0 , denoted R_N . The horizontal slownesses corresponding to the rays are $p_m = \sin \Theta_m / V_m$ and $p_0 = \sin \Theta_0 / V_0$. The ray and slowness at x_m are depicted in Figure 1b, where those at x_0 were omitted for simplicity.

For our derivation, we assume that all distances are infinitesimal. Under this assumption, the medium is still anisotropic but homogeneous within the considered vicinity. In particular, this means that the ray (group) and phase directions do not change along the ray. Furthermore, the operator derived in this section is a 2D expression. Therefore, waves are assumed to propagate in the $x - z$ -plane. The 3D situation will be discussed further below.

In order to relate the derivatives in the Taylor expansion 4 to the quantities we just introduced, we use the law of sines for the triangle in Figure 1c. The angles and the lengths of their opposing sides define the geometry we need for the sought-for relation. They are

- a.) the angle $90^\circ - \vartheta_m$ and the distance between the two rays, approximated by the arclength $R_N \Delta \Theta_m = R_N (\Theta_m - \Theta_0)$ (note that the distance between the rays is calculated by the phase angles, not the ray angles, because unlike the slowness vectors the rays are not perpendicular to the wavefront),
- b.) the angle $\Theta_0 + \Delta \Theta_m / 2$ and the distance $v_m \Delta t_m = v_m (t(x_m) - t(x_0))$,
- a.) the angle $90^\circ + \psi_m + \Delta \Theta_m / 2$ and the distance $\Delta x_m = x_m - x_0$.

Using these, the law of sines provides the following relationships,

$$\frac{\sin(90^\circ + \psi_m + \Delta \Theta_m / 2)}{\Delta x_m} = \frac{\sin(\Theta_0 + \Delta \Theta_m / 2)}{v_m \Delta t_m} = \frac{\sin(90^\circ - \vartheta_m)}{R_N \Delta \Theta_m} \quad , \quad (5)$$

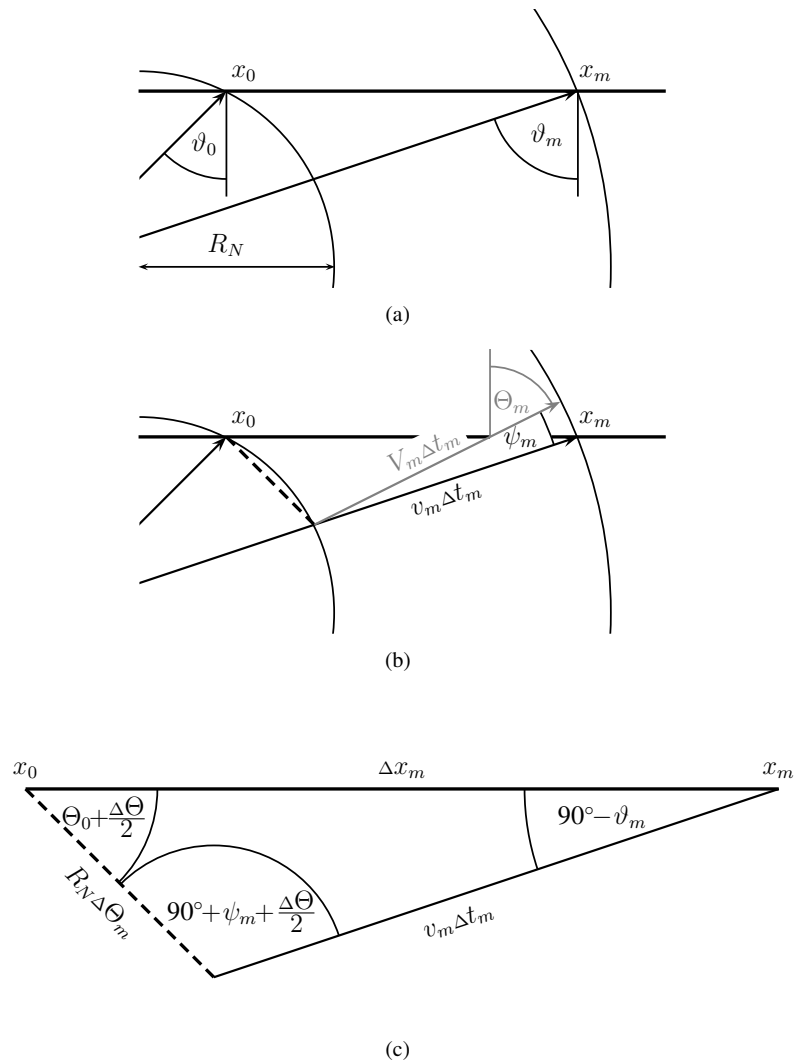


Figure 1: (a) Two zero-offset rays and their associated wavefronts arriving at locations x_m and x_0 in the registration surface. Owing to the anisotropy the rays are not perpendicular to the wavefronts. The angles ϑ_m and ϑ_0 are ray angles. The radius of curvature of the incident wavefront at x_0 is R_N . (b) Zero-offset rays (black), slownesses (gray), and wavefronts. The angle Θ_m is the phase angle. The angle ψ_m lies between the ray and the slowness vector. Since we assume that the medium is locally homogeneous, all angles and velocities remain constant along the rays. The dashed line approximates the wavefront emerging at x_0 . (c) Triangle with distances and angles used for the law of sines (see text). The angle $\Delta \Theta/2$ lies between the arc and the dashed line in (b).

or, applying $\sin(90^\circ \pm \alpha) = \cos \alpha$,

$$\frac{\cos(\psi_m + \Delta\Theta_m/2)}{\Delta x_m} = \frac{\sin(\Theta_0 + \Delta\Theta_m/2)}{v_m \Delta t_m} = \frac{\cos \vartheta_m}{R_N \Delta\Theta_m} \quad (6)$$

With

$$\frac{\Delta t_m}{\Delta x_m} = \frac{\sin(\Theta_0 + \Delta\Theta_m/2)}{v_m \cos(\psi_m + \Delta\Theta_m/2)} \quad (7)$$

we obtain

$$\left. \frac{\partial t_m}{\partial x_m} \right|_{x_0} = \lim_{x_m \rightarrow x_0} \frac{\Delta t_m}{\Delta x_m} = \frac{\sin \Theta_0}{v_0 \cos \psi_0} \quad (8)$$

Substituting the relationship between phase and group velocity, $V = v \cos \psi$ (e.g., Tsvankin, 2001, see also Figure 1b), we find that this derivative is, as expected, the horizontal slowness p_0 at x_0 ,

$$p_0 = \left. \frac{\partial t_m}{\partial x_m} \right|_{x_0} = \frac{\sin \Theta_0}{V_0} \quad (9)$$

Taking into account that the situation depicted in Figure 1 that led us to this result is a one-way process, whereas the Taylor expansion in Equation 4 is a two-way process, we find the first-order derivative in Equation 4 to be

$$\left. \frac{\partial t}{\partial x_m} \right|_{x_0, h=0} = 2 \left. \frac{\partial t_m}{\partial x_m} \right|_{x_0} = 2 \frac{\sin \Theta_0}{V_0} \quad (10)$$

For the determination of the second-order derivative of the traveltime with respect to x_m , we differentiate the general expression for the horizontal slowness, $p = \sin \Theta / V$, i.e.,

$$\begin{aligned} \left. \frac{\partial^2 t_m}{\partial x_m^2} \right|_{x_0} &= \left. \frac{\partial p_m}{\partial x_m} \right|_{x_0} \\ &= \left[\frac{1}{V_m^2} \left(V_m \frac{\partial \sin \Theta_m}{\partial x_m} - \sin \Theta_m \frac{\partial V_m}{\partial x_m} \right) \right]_{x_0} \\ &= \left[\frac{1}{V_m^2} \left(V_m \cos \Theta_m \frac{\partial \Theta_m}{\partial x_m} - \sin \Theta_m \frac{\partial V_m}{\partial \Theta_m} \frac{\partial \Theta_m}{\partial x_m} \right) \right]_{x_0} \end{aligned} \quad (11)$$

This expression contains two unknown partial derivatives. One of them can be resolved by the relationship between the phase velocity and the vertical component v_z of the group velocity. With (e.g., Tsvankin, 2001)

$$v_z = v \cos \vartheta = V \cos \Theta - \frac{\partial V}{\partial \Theta} \sin \Theta \quad (12)$$

we find that

$$\frac{\partial V}{\partial \Theta} = \frac{V \cos \Theta - v \cos \vartheta}{\sin \Theta} \quad (13)$$

For the remaining unknown partial derivative in Equation 11, we can again apply the law of sines 6, where

$$\frac{\Delta\Theta_m}{\Delta x_m} = \frac{\cos \vartheta_m}{R_N \cos(\psi_m + \Delta\Theta_m/2)} \quad (14)$$

leads to

$$\left. \frac{\partial \Theta_m}{\partial x_m} \right|_{x_0} = \lim_{x_m \rightarrow x_0} \frac{\Delta\Theta_m}{\Delta x_m} = \frac{\cos \vartheta_0}{R_N \cos \psi_0} \quad (15)$$

Substituting 13 and 15 into 11, the second-order derivative 11 becomes

$$\left. \frac{\partial^2 t_m}{\partial x_m^2} \right|_{x_0} = \frac{\cos^2 \vartheta_0}{v_0 \cos^3 \psi_0 R_N} \quad (16)$$

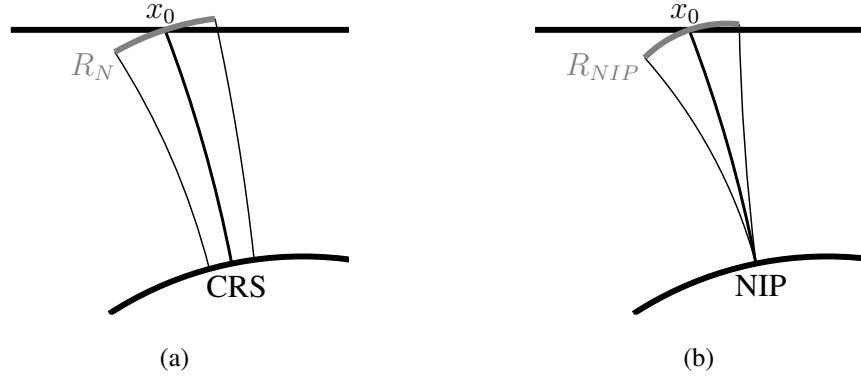


Figure 2: Wavefront (gray) curvatures in the zero-offset CRS: (a) R_N is the radius of curvature of the so-called normal or N-wavefront that is generated by a fictitious exploding reflector element, denoted common reflection surface (CRS), around the normal incidence point (NIP, see b). It corresponds to a zero-offset experiment. Note that normal incidence refers to the slowness, not ray, direction in case of anisotropy. (b) R_{NIP} is the radius of curvature of the so-called NIP-wavefront that is generated by a fictitious point source in the NIP. It corresponds to a common midpoint (CMP) experiment.

and, therefore,

$$\left. \frac{\partial^2 t}{\partial x_m^2} \right|_{x_0, h=0} = 2 \left. \frac{\partial^2 t_m}{\partial x_m^2} \right|_{x_0} = 2 \frac{\cos^2 \vartheta_0}{v_0 \cos^3 \psi_0 R_N} . \quad (17)$$

Note that this second-order derivative can also be expressed by the phase angle and phase velocity; however, the expression is more compact in terms of ray/group properties.

Before we turn to the derivation of the remaining term in the Taylor expansion 4, let us take a closer look at the wavefront curvature radius R_N in Figure 2a. It describes a fictitious wavefront that is generated by an exploding reflector element, the so-called common reflection surface (CRS). It is commonly referred to as the normal wavefront (Tygel et al., 1997) and measured by the zero-offset experiment described in Figure 2a.

If we now consider a common-midpoint (CMP) experiment, we find a corresponding fictitious wavefront, the normal-incident-point (NIP) wavefront, generated by a point source in the NIP as depicted in Figure 2b. As for the derivation of the second-order derivative with respect to x_m , i.e., for the zero-offset experiment, we can follow the same steps for the second-order derivative with respect to h . In the latter case, we have the CMP experiment, and all we need to do is replace R_N in Equation 17 with the radius of the NIP wavefront, R_{NIP} , and x_m with h . We obtain

$$\left. \frac{\partial^2 t}{\partial h^2} \right|_{x_0, h=0} = 2 \frac{\cos^2 \vartheta_0}{v_0 \cos^3 \psi_0 R_{NIP}} . \quad (18)$$

In conclusion, the anisotropic CRS operator for the zero-offset case is given by

$$t^2 = \left(t_0 + 2 \frac{\sin \Theta_0}{V_0} \Delta x_m \right)^2 + 2 t_0 \frac{\cos^2 \vartheta_0}{v_0 \cos^3 \psi_0} \left(\frac{\Delta x_m^2}{R_N} + \frac{h^2}{R_{NIP}} \right) . \quad (19)$$

In the following section, we use this result and the work by Vanelle and Gajewski (2002) to derive the extension to the finite-offset situation.

Anisotropic CRS for 2D finite offset

In order to derive the anisotropic finite-offset operator, we use the traveltimes for an arbitrary source-receiver combination (s, g) in the vicinity of an expansion point at (s_0, g_0) in the hyperbolic expression suggested by Vanelle and Gajewski (2002),

$$t^2(s, g) = (t_0 + p_g \Delta g - p_s \Delta s)^2 + t_0 (G \Delta g^2 - S \Delta s^2 - 2 N \Delta s \Delta g) , \quad (20)$$

where $\Delta s = s - s_0$ and $\Delta g = g - g_0$ are the distances of the source and receiver positions to the expansion point, respectively, and t_0 is the traveltimes in the expansion point, i.e., $t_0 = t(s_0, g_0)$. The coefficients in Equation 20 are the first- and second-order derivatives of the traveltimes with respect to source and receiver coordinates. Namely, the first-order derivatives,

$$p_s = -\left. \frac{\partial t}{\partial s} \right|_{s_0, g_0} \quad \text{and} \quad p_g = \left. \frac{\partial t}{\partial g} \right|_{s_0, g_0}, \quad (21)$$

are the horizontal slownesses at the source and receiver, respectively. The second-order derivatives are given by

$$S = -\left. \frac{\partial^2 t}{\partial s^2} \right|_{s_0, g_0}, \quad G = \left. \frac{\partial^2 t}{\partial g^2} \right|_{s_0, g_0}, \quad \text{and} \quad N = -\left. \frac{\partial^2 t}{\partial s \partial g} \right|_{s_0, g_0}. \quad (22)$$

In midpoint and half-offset coordinates (x_m, h) , with $x_m = (g + s)/2$, $h = (g - s)/2$, and $\Delta h = h - h_0$, $\Delta x_m = x_m - x_0$, Equation 20 reads

$$\begin{aligned} t^2(x_m, h) &= (t_0 + (p_g - p_s) \Delta x_m + (p_g + p_s) \Delta h)^2 \\ &\quad + t_0 \left((G - S - 2N) \Delta x_m^2 + (G - S + 2N) \Delta h^2 + 2(G + S) \Delta x_m \Delta h \right). \end{aligned} \quad (23)$$

Again, in the zero-offset situation for monotypic waves, all traveltimes expressions given above must be symmetric with respect to interchanging the source and receiver, i.e., changing the sign of h . Therefore, the following relations apply:

$$p_g = -p_s \quad \text{and} \quad G = -S. \quad (24)$$

Furthermore, we have $h_0 = 0$ and, therefore, $\Delta h = h$. In conclusion, Equation 23 simplifies. It can be expressed either in terms of (p_s, S, N) or (p_g, G, N) , i.e.,

$$t^2(x_m, h) = (t_0 - 2p_s \Delta x_m)^2 + 2t_0 \left((-S - N) \Delta x_m^2 + (-S + N) h^2 \right) \quad (25)$$

and

$$t^2(x_m, h) = (t_0 + 2p_g \Delta x_m)^2 + 2t_0 \left((G - N) \Delta x_m^2 + (G + N) h^2 \right). \quad (26)$$

We now consider the zero-offset CRS operator, Equation 19. Comparing the coefficients in Equations 26 and 25 with those in 19, we find that the parameters are related by

$$\begin{aligned} \frac{\cos^2 \vartheta_0}{v_0 \cos^3 \psi_0 R_N} &= G - N = -S - N, \\ \frac{\cos^2 \vartheta_0}{v_0 \cos^3 \psi_0 R_{NIP}} &= G + N = -S + N, \\ \frac{\sin \Theta_0}{V_0} &= p_g = -p_s. \end{aligned} \quad (27)$$

In a formally identical fashion to the zero-offset parameters in Equation 27, we introduce according finite-offset parameters

$$\begin{aligned} \frac{\cos^2 \vartheta_g}{v_g \cos^3 \psi_g R_g^{CO}} &= G - N, & \frac{\cos^2 \vartheta_s}{v_s \cos^3 \psi_s R_s^{CO}} &= -S - N, \\ \frac{\cos^2 \vartheta_g}{v_g \cos^3 \psi_g R_g^{CMP}} &= G + N, & \frac{\cos^2 \vartheta_s}{v_s \cos^3 \psi_s R_s^{CMP}} &= -S + N, \\ \frac{\sin \Theta_g}{V_g} &= p_g, & \frac{\sin \Theta_s}{V_s} &= -p_s. \end{aligned} \quad (28)$$

These parameters are, like those in the zero-offset case, angles and curvatures of fictitious wavefronts (see Figure 3). In contrast to the zero-offset case, the phase directions are no longer normal to the interface, and therefore a normal incidence point does not exist. Furthermore, the zero-offset parameters describe a one-way process. In the finite-offset case, where the down-going and up-going rays no longer coincide, a two-way process has to be considered. Our choice of parameters accounts for this fact. In conclusion, our operator reads

$$\begin{aligned}
t^2(x_m, h) = & \left[t_0 + \left(\frac{\sin \Theta_g}{V_g} + \frac{\sin \Theta_s}{V_s} \right) \Delta x_m + \left(\frac{\sin \Theta_g}{V_g} - \frac{\sin \Theta_s}{V_s} \right) \Delta h \right]^2 \\
& + t_0 \left[\frac{\cos^2 \vartheta_g}{v_g \cos^3 \psi_g R_g^{CO}} + \frac{\cos^2 \vartheta_s}{v_s \cos^3 \psi_s R_s^{CO}} \right] \Delta x_m^2 \\
& + t_0 \left[\frac{\cos^2 \vartheta_g}{v_g \cos^3 \psi_g R_g^{CMP}} + \frac{\cos^2 \vartheta_s}{v_s \cos^3 \psi_s R_s^{CMP}} \right] \Delta h^2 \\
& + 2 t_0 \left[\frac{\cos^2 \vartheta_g}{v_g \cos^3 \psi_g R_g^{CMP}} - \frac{\cos^2 \vartheta_s}{v_s \cos^3 \psi_s R_s^{CMP}} \right] \Delta x_m \Delta h \quad . \quad (29)
\end{aligned}$$

Note that the mixed term could also be expressed by the $R_{s,g}^{CO}$ because

$$\frac{\cos^2 \vartheta_g}{v_g \cos^3 \psi_g R_g^{CMP}} - \frac{\cos^2 \vartheta_s}{v_s \cos^3 \psi_s R_s^{CMP}} = \frac{\cos^2 \vartheta_g}{v_g \cos^3 \psi_g R_g^{CO}} - \frac{\cos^2 \vartheta_s}{v_s \cos^3 \psi_s R_s^{CO}} \quad . \quad (30)$$

However, it is known from the isotropic zero-offset case that the parameter R_N behaves less stable than R_{NIP} . This behaviour also applies to the $R_{s,g}^{CO}$ because these correspond to R_N in the zero-offset case. Therefore, we prefer to express the mixed term in Equation 29 by the $R_{s,g}^{CMP}$. In practice, midpoint apertures, i.e., distances Δx_m , are chosen small. Therefore, the potential instability of $R_{s,g}^{CO}$ has limited impact on the stack since it occurs only in the second order term for Δx_m^2 .

For applications like NIP-wave and diffraction tomography (Duveneck, 2004; Bauer et al., 2016), $R_{s,g}^{CO}$ are not required. If all parameters in 29 are determined, the equality 30 could be used as a means for quality control for the parameters $R_{s,g}^{CO}$.

A finite offset operator with according parameters for the isotropic case was introduced by Zhang et al. (2001). The wavefront curvature parameters $R_{s,g}^{CMP}$ and $R_{s,g}^{CO}$ in 28 were adopted from that work, where their names refer to the CMP and common-offset (CO) experiments. The operator by Zhang et al. (2001) is expressed by the two curvatures $K_{s,g}^{CMP} = 1/R_{s,g}^{CMP}$ and a third wavefront curvature, K^{CS} that is measured at the receiver in a common-source (CS) experiment. This parameterisation leads to a slightly less appealing look of their operator because the individual terms lose the symmetry in the parameters that our expression displays. Furthermore, use of the $R_{s,g}^{CO}$ as opposed to K^{CS} avoids potential issues arising from the reflection point dispersal associated with a common-shot experiment. Owing to these reasons, we prefer to express the anisotropic operator as given by 29.

In the following, we extend the anisotropic finite-offset CRS operator 29 to the general three-dimensional case.

Anisotropic CRS for 3D finite offset

Whereas in two dimensions a derivation of the anisotropic operator from the laws of geometry was easily feasible, it is not as simple to visualise in the 3D case. We can, however, derive the 3D operator by combining our results from the 2D situation with the ray method.

In this section, we need to distinguish between vectors with two or three components as well as between 2×2 and 3×3 matrices. Therefore, we denote two-component vectors and 2×2 matrices with a bold font, e.g., vector \mathbf{a} and matrix \mathbf{A} . Three-component vectors and 3×3 matrices are also printed in bold, but carry a hat in addition, e.g., $\hat{\mathbf{b}}$ and matrix $\hat{\mathbf{B}}$. Scalars are printed in regular font.

In general, the operator will retain the same form as in two dimensions. We need to replace the scalars describing coordinates and slownesses with vectors, and the scalar wavefront curvatures become matrices,

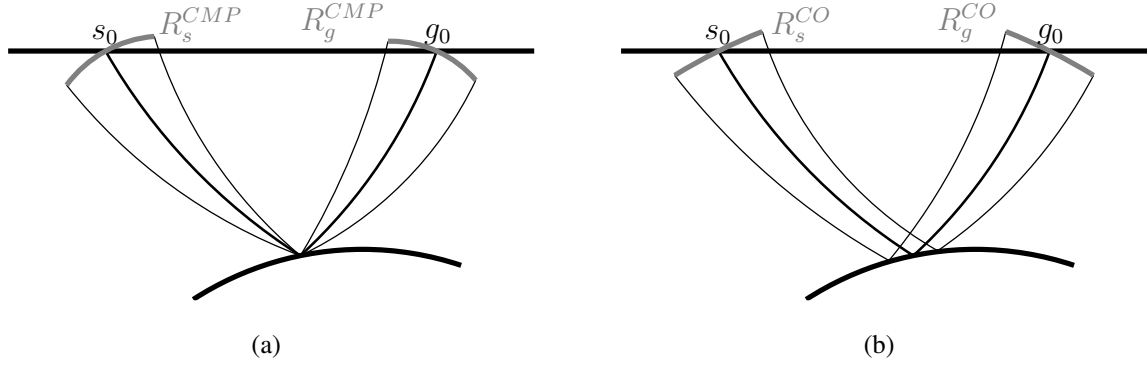


Figure 3: Wavefront (gray) curvatures in the finite-offset CRS: (a) R_s^{CMP} and R_g^{CMP} are the radii of curvature of two fictitious wavefronts that are measured at the source and receiver, respectively, for a CMP experiment. (b) R_s^{CO} and R_g^{CO} are the radii of curvature of two fictitious wavefronts that are measured at the source and receiver, respectively, for a finite-offset experiment.

resulting in

$$\begin{aligned}
 t^2(\mathbf{x}_m, \mathbf{h}) &= [t_0 + (\mathbf{p}_g - \mathbf{p}_s) \Delta \mathbf{x}_m^\top + (\mathbf{p}_g + \mathbf{p}_s) \Delta \mathbf{h}^\top]^2 \\
 &\quad + t_0 \Delta \mathbf{x}_m [\underline{\mathbf{M}}_g^{CO} - \underline{\mathbf{M}}_s^{CO}] \Delta \mathbf{x}_m^\top \\
 &\quad + t_0 \Delta \mathbf{h} [\underline{\mathbf{M}}_g^{CMP} - \underline{\mathbf{M}}_s^{CMP}] \Delta \mathbf{h}^\top \\
 &\quad + 2 t_0 \Delta \mathbf{x}_m [\underline{\mathbf{M}}_g^{CMP} + \underline{\mathbf{M}}_s^{CMP}] \Delta \mathbf{h}^\top, \quad (31)
 \end{aligned}$$

where the 2×2 matrices $\underline{\mathbf{M}}$ are second-order derivatives of the traveltimes in the acquisition surface at the source and receiver position for the respective measurement configurations. As in 2D, the following relationship holds,

$$\underline{\mathbf{M}}_g^{CMP} + \underline{\mathbf{M}}_s^{CMP} = \underline{\mathbf{M}}_g^{CO} + \underline{\mathbf{M}}_s^{CO}. \quad (32)$$

The first-order derivatives follow immediately as the horizontal slowness components, i.e.,

$$\mathbf{p}_s^\top = -\frac{\sin \Theta_s}{V_s} \begin{pmatrix} \cos \Phi_s \\ \sin \Phi_s \end{pmatrix} \quad \text{and} \quad \mathbf{p}_g^\top = \frac{\sin \Theta_g}{V_g} \begin{pmatrix} \cos \Phi_g \\ \sin \Phi_g \end{pmatrix}, \quad (33)$$

where the angles Φ_s and Φ_g describe the azimuth of the slowness vectors. For the second-order derivatives, we find in the literature (e.g., Höcht, 2002; Müller, 2007) for the 3D isotropic zero-offset attributes that

$$\underline{\mathbf{M}} = \frac{1}{u} \underline{\mathbf{H}} \underline{\mathbf{K}} \underline{\mathbf{H}}^\top, \quad (34)$$

which can be used to express both $\underline{\mathbf{M}}_N$ and $\underline{\mathbf{M}}_{NIP}$. As the same form applies to all matrices $\underline{\mathbf{M}}$, we will from now on omit the indices for the type of experiment and position.

In Equation 34, $\underline{\mathbf{K}}$ is a symmetric wavefront curvature matrix in ray-centred coordinates (according to Müller, 2007) or wavefront-orthonormal coordinates (according to Höcht, 2002). In ray-centred coordinates (rcc), the unit vector of the third axis, $\hat{\mathbf{e}}_3^{rcc}$, is given by the ray direction, i.e.,

$$\hat{\mathbf{e}}_3^{rcc} = \frac{\hat{\mathbf{v}}}{|\hat{\mathbf{v}}|}, \quad (35)$$

whereas in wavefront-orthonormal coordinates (woc)

$$\hat{\mathbf{e}}_3^{woc} = \frac{\hat{\mathbf{p}}}{|\hat{\mathbf{p}}|}, \quad (36)$$

i.e., the unit vector of the third axis, \hat{e}_3^{woc} , points in the direction of the slowness. Matrix $\underline{\mathbf{H}}$ is the upper left 2×2 submatrix of the transformation matrix from either of these coordinates to the acquisition system. The quantity u is a near-surface velocity that is not further specified.

In isotropic media we need not distinguish between phase and ray (group) velocity because $v = V \equiv u$. Furthermore, wavefront-orthonormal and ray-centred coordinates coincide. This is, however, not the case in anisotropic media, where the according transformation cannot be achieved by a simple 2×2 matrix. A quick look at the 2D situation illustrates this: In the previous section, we have shown that

$$M = \frac{K \cos^2 \vartheta}{v \cos^3 \psi} = \frac{K \cos^2 \vartheta}{V \cos^2 \psi} \quad , \quad (37)$$

where R was substituted with $1/K$. If $\underline{\mathbf{H}}$ described the transformation between acquisition and ray-centred coordinates, Equation 34 would lead to

$$M = \frac{K \cos^2 \vartheta}{v} \quad (38)$$

with $u = v$ or

$$M = \frac{K \cos^2 \vartheta}{V} = \frac{K \cos^2 \vartheta}{v \cos \psi} \quad (39)$$

with $u = V$. Similarly, if $\underline{\mathbf{H}}$ described the transformation between acquisition and wavefront-orthonormal coordinates, we would obtain

$$M = \frac{K \cos^2 \Theta}{v} \quad (40)$$

with $u = v$ or

$$M = \frac{K \cos^2 \Theta}{V} = M = \frac{K \cos^2 \Theta}{v \cos \psi} \quad (41)$$

with $u = V$. Whereas these solutions coincide in the special case of isotropy where $\psi = 0$, neither one yields the correct result 37 in the anisotropic situation.

In order to find a correct representation for anisotropic media, we refer to Červený (2001) for the following considerations.

The relationship between a matrix $\underline{\mathbf{M}}^{woc}$ and the symmetric wavefront curvature matrix $\underline{\mathbf{K}}$ is given by

$$\underline{\mathbf{K}} = V \underline{\mathbf{M}}^{woc} \quad , \quad (42)$$

where V denotes (as before) the phase velocity and $\underline{\mathbf{M}}^{woc}$ is the upper left 2×2 submatrix of the 3×3 matrix $\hat{\underline{\mathbf{M}}}^{woc}$ that is defined as the Hessian of the traveltimes in wavefront-orthonormal coordinates x_i^{woc} ,

$$\hat{M}_{ij}^{woc} = \frac{\partial^2 t}{\partial x_i^{woc} \partial x_j^{woc}} \quad , \quad (43)$$

or

$$\hat{\underline{\mathbf{M}}}^{woc} = \begin{pmatrix} \underline{\mathbf{M}}^{woc} & M_{13}^{woc} \\ & M_{23}^{woc} \\ M_{13}^{woc} & M_{23}^{woc} & M_{33}^{woc} \end{pmatrix} \quad . \quad (44)$$

Expressed by the curvature matrix $\underline{\mathbf{K}}$ and the ray velocity vector in wavefront-orthonormal coordinates, \mathbf{v}^{woc} , for the locally homogeneous medium we consider matrix $\hat{\underline{\mathbf{M}}}^{woc}$ becomes

$$\hat{\underline{\mathbf{M}}}^{woc} = \frac{1}{V^3} \begin{pmatrix} V^2 \underline{\mathbf{K}} & -V v_J^{woc} M_{1J}^{woc} \\ & -V v_J^{woc} M_{2J}^{woc} \\ -V v_J^{woc} M_{1J}^{woc} & -V v_J^{woc} M_{2J}^{woc} & -V^2 v_I^{woc} v_J^{woc} M_{IJ}^{woc} \end{pmatrix} \quad , \quad (45)$$

where summation convention is applied with indices I and J taking values 1 and 2. The latter relationship can be derived from the definition of the slowness vector $\hat{\mathbf{p}}$ as the gradient of the traveltimes t and the fact that the scalar product of the group velocity and slowness vectors equals one in any coordinate system, i.e.,

$$\hat{\mathbf{p}} \cdot \hat{\mathbf{v}} = \vec{\nabla} t \cdot \hat{\mathbf{v}} = 1 \quad , \quad (46)$$

or, component-wise,

$$\frac{\partial t}{\partial x} v_x + \frac{\partial t}{\partial y} v_y + \frac{\partial t}{\partial z} v_z = 1 \quad . \quad (47)$$

The gradient of this expression is zero. Assuming a locally homogeneous medium and considering wavefront-orthonormal coordinates, where $v_z^{woc} = V$, we find that

$$\begin{aligned} M_{xx}^{woc} v_x^{woc} + M_{xy}^{woc} v_y^{woc} + M_{xz}^{woc} v_z^{woc} &= 0 \quad , \\ M_{yx}^{woc} v_x^{woc} + M_{yy}^{woc} v_y^{woc} + M_{yz}^{woc} v_z^{woc} &= 0 \quad , \\ M_{zx}^{woc} v_x^{woc} + M_{zy}^{woc} v_y^{woc} + M_{zz}^{woc} v_z^{woc} &= 0 \quad , \end{aligned} \quad (48)$$

which provides Equation 45.

With the transformation matrix $\hat{\mathbf{H}}$ from wavefront-orthonormal coordinates to the acquisition system,

$$\hat{H}_{ij} = \frac{\partial x_i}{\partial x_j^{woc}} = \frac{\partial x_j^{woc}}{\partial x_i} \quad , \quad (49)$$

we can now determine the 3×3 Hessian matrix of the traveltimes, $\hat{\mathbf{M}}$, in the acquisition system with $\hat{\mathbf{e}}_3$ oriented in z -direction by

$$\hat{\mathbf{M}} = \hat{\mathbf{H}} \hat{\mathbf{M}}^{woc} \hat{\mathbf{H}}^\top \quad . \quad (50)$$

Applied to each experiment (CMP, CO) at the source and receiver coordinates, the upper left 2×2 submatrices of the according matrices $\hat{\mathbf{M}}$ are the sought-after matrices \mathbf{M} in the operator 31.

For illustration, we show that this procedure leads to the correct result in the 2D case. With the transformation matrix

$$\mathbf{H} = \begin{pmatrix} \cos \Theta & \sin \Theta \\ -\sin \Theta & \cos \Theta \end{pmatrix} \quad (51)$$

and the ray velocity vector in the acquisition and wavefront-orthonormal coordinates,

$$\begin{aligned} \mathbf{v} &= v (\sin \vartheta, \cos \vartheta) \\ \mathbf{v}^{woc} &= v (\sin(\vartheta - \Theta), \cos(\vartheta - \Theta)) \\ &= v (\sin \psi, \cos \psi) \end{aligned} \quad (52)$$

the matrix \mathbf{M}^{woc} becomes

$$\mathbf{M}^{woc} = \frac{K}{v \cos^3 \psi} \begin{pmatrix} \cos^2 \psi & -\sin \psi \cos \psi \\ -\sin \psi \cos \psi & \sin^2 \psi \end{pmatrix} \quad , \quad (53)$$

where $V = v \cos \psi$ was substituted. After carrying out the coordinate transformation, we find that

$$\begin{aligned} M &= \frac{K}{v \cos^3 \psi} (\cos^2 \Theta \cos^2 \psi + \sin^2 \Theta \sin^2 \psi - 2 \sin \Theta \sin \psi \cos \Theta \cos \psi) \\ &= \frac{K}{v \cos^3 \psi} (\cos \Theta \cos \psi - \sin \Theta \sin \psi)^2 \\ &= \frac{K \cos^2(\Theta + \psi)}{v \cos^3 \psi} \\ &= \frac{K \cos^2 \vartheta}{v \cos^3 \psi} \quad . \end{aligned} \quad (54)$$

This is the correct result that we also obtained from the 2D derivation.

Now that we have established the theory, we demonstrate our results with numerical examples in the following section.

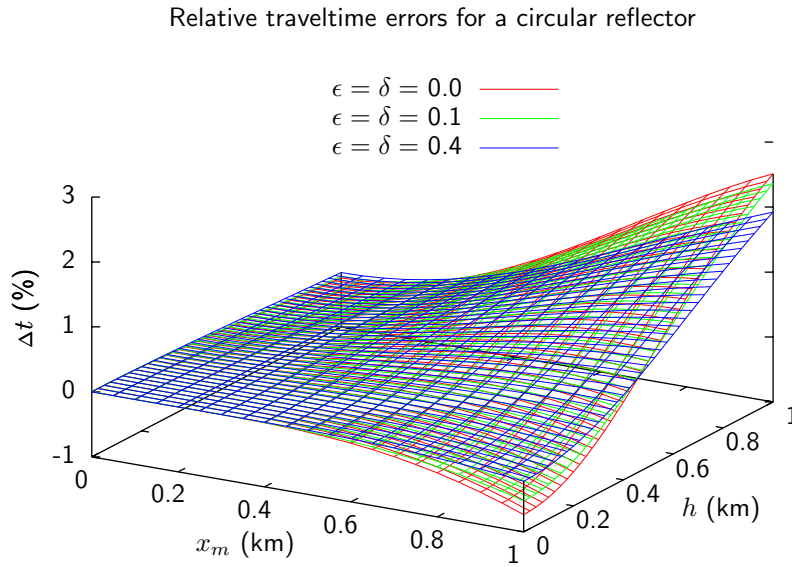


Figure 4: Relative traveltimes errors of the anisotropic zero-offset CRS operator for a circular reflector with a radius of 1 km in a homogeneous medium with elliptical anisotropy. The CMP under consideration is located at $x_0 = 0.2$ km.

NUMERICAL EXAMPLES

In this section, we demonstrate the accuracy of the 2D zero-offset operator. Since the performance of the isotropic counterpart in 2D and 3D is well established and the shape of the operator is the same, we have decided to restrict the examination to examples with a curved reflector and a point diffractor in a homogeneous anisotropic medium with elliptical symmetry. The reason why we chose a medium with elliptical symmetry is that this is the only anisotropic medium in which we can compute all parameters, i.e., all velocities and angles as well as the wavefront curvatures, analytically.

It is known from the isotropic CRS that its accuracy decreases with increasing reflector curvature (e.g., Vanelle et al., 2010). It performs worst for diffractions because diffraction traveltimes are better described by a double square root expression than by a hyperbola. We found the same general behaviour also for the anisotropic CRS. Since it can be shown that the operator 29 coincides with the exact traveltimes for the case of an inclined or horizontal planar reflector in a homogeneous background medium with elliptical anisotropy, we present only results for a circular reflector and for a point diffractor.

The centre of the circular reflector with a radius of 1 km is located at (0;2) km. The point diffractor is located at (0;1) km. The background medium has a vertical velocity of 2 km and we have considered values for $\epsilon = \delta = 0$ (i.e., isotropy), $\epsilon = \delta = 0.1$ (weak anisotropy), and $\epsilon = \delta = 0.4$. Reference traveltimes were generated using the NORSAR ray modelling software for the reflections and analytically for the diffractions. The expansion point was taken at $x_0 = 0.2$ km in all cases.

Figure 4 shows the relative errors of the reflection traveltimes for midpoint deviations of up to 0.8 km and an offset-to-target ratio of two. Keeping in mind that in stacking, midpoint deviations as well as offset-to-target ratios are in practice smaller than the shown range, we find the resulting accuracy satisfying. The isotropic as well as the anisotropic case display the same magnitude of accuracy.

In the diffraction case displayed in Figure 5, we observe that, as expected, the accuracy is slightly lower than for the reflection. The overall accuracy confirms that the operator leads to reasonable results.

DISCUSSION

In the previous sections, we have derived the anisotropic extension of the CRS operator and verified it with examples. In this section, we briefly address several points that arose during our investigation.

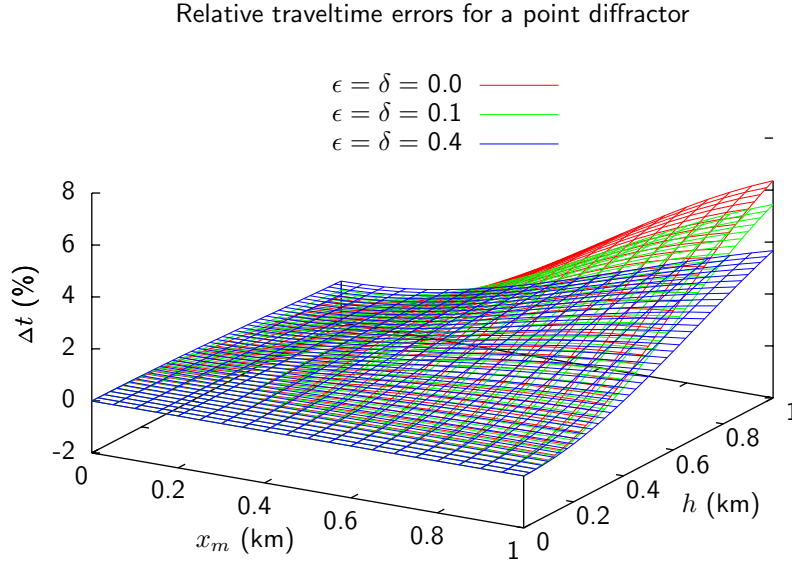


Figure 5: Relative traveltimes errors of the anisotropic zero-offset CRS operator for a point diffractor in a homogeneous medium with elliptical anisotropy. The CMP under consideration is located at $x_0 = 0.2$ km.

Instead of three parameters, namely two wavefront curvature radii and an angle, and the near-surface velocity in the 2D isotropic zero-offset case, our anisotropic zero-offset operator requires four parameters and a velocity. Although the operator in Equation 19 is expressed in terms of two radii of wavefront curvature, R_N and R_{NIP} , three angles Θ_0 , ϑ_0 , ψ_0 , and two velocities v_0 , V_0 , only three of the latter five quantities are independent. With the relationships

$$V_0 = v_0 \cos \psi_0 = v_0 \cos (\vartheta_0 - \Theta_0) \quad (55)$$

it is possible to express the operator in terms of only three of the above-mentioned five quantities, namely, one velocity and two angles, which can be chosen at will. We have expressed the first-order derivatives in Equation 19 by the phase angle and phase velocity because these describe the slowness. For the second-order terms, we use the ray velocity and angle as well as angle ψ_0 because these provide the most compact expression.

As already suggested in the introduction, the determination of all parameters in the anisotropic case by stacking is not generally possible unless model assumptions are made. For the stack itself, this is not an issue because the shape of the operator is the same as in the isotropic case. If we wish to apply the parameters, e.g., for NIP-wave (Duveneck, 2004) or diffraction tomography (Bauer et al., 2016), model assumptions must be made in any event. These assumptions can then be used to calculate the anisotropic parameters from the three parameters obtained during the stack. Furthermore, in many practical applications, e.g., in a marine acquisition, the near-surface region is or is assumed to be isotropic.

Most established anisotropic traveltimes formulations (e.g., Tsvankin and Thomsen, 1994) consider non-hyperbolic moveout. This is necessary as soon as medium to far offsets need to be taken into account. In contrast, our operator was derived for application within the hyperbolic limit, i.e., under the short-spread assumption. Within this assumption, the operator provides good results. Outside this limit, the accuracy generally decreases with increasing offset and midpoint displacement. However, this is also the case if the medium is isotropic as soon as heterogeneities are present. The examples in Figures 4 and 5 in the previous section demonstrate this. In conclusion, as long as the apertures are chosen in accordance with the assumption of short spread, a hyperbolic operator will provide good results.

CONCLUSIONS

We have derived a CRS-type multiparameter operator for anisotropic media in three dimensions. The operator is valid for finite offset configuration with zero offset as a special case. It does not make any model assumptions. Numerical examples demonstrate that the accuracy of the operator is of the same order as for isotropic media.

Like its isotropic counterpart, the anisotropic operator is parameterised in terms of angles and wavefront curvatures. To account for the anisotropy, the distinction between ray (group) and phase angles and velocities must be considered. In the zero-offset case, the anisotropic operator requires an additional angle that describes the deviation between group and phase direction. For finite offsets, two additional angles are required.

If no model assumptions are made, only three of the four parameters in the 2D zero-offset case can be determined by stacking and semblance analysis because the shape of the operator remains the same as for isotropy. This is an advantage because it means that the stack result does not depend on the presence or absence of anisotropy. If, on the other hand, model assumptions are made, the model provides the necessary relations between the wavefield parameters. In that case, all parameters can be determined by stacking.

In many applications, model assumptions enter only after the stacking. In these further processing steps, neglecting potential anisotropy can lead to errors, e.g. if velocity tomography is performed based on isotropic wavefield parameters if the medium is anisotropic. With our new parameterisation, anisotropic wavefield parameters can be applied as soon as an anisotropic model is considered.

Furthermore, we like to think that this new formulation enhances our understanding of surface-measured wavefield properties in arbitrary three-dimensional anisotropic media.

ACKNOWLEDGEMENTS

We are grateful to the members of the Applied Seismics Group in Hamburg for continuous and inspiring discussion, in particular to Benjamin Schwarz, Jan Walda, Sophia Wißmath, and Boris Kashtan. Further thanks go to Jan Walda for proof-reading. Korbinian Sager generated traveltimes tables using NORSAR ray modelling software. This work was partially supported by the sponsors of the Wave Inversion Technology (WIT) consortium.

REFERENCES

- Bauer, A., Schwarz, B., and Gajewski, D. (2016). Improving the resolution of wavefront tomography by utilizing diffractions. *86th Annual International Meeting, SEG, Expanded Abstracts*, pages 5296–5301.
- Baykulov, M. and Gajewski, D. (2009). Prestack seismic data enhancement with partial common reflection surface (CRS) stack. *Geophysics*, 74:V49–V58.
- Červený, V. (2001). *Seismic Ray Theory*. Cambridge University Press.
- Dell, S. and Gajewski, D. (2011). Common-reflection-surface-based workflow for diffraction imaging. *Geophysics*, 76:S187–S195.
- Dümmong, S. and Gajewski, D. (2008). A multiple suppression method via CRS attributes. *78th Annual International Meeting, SEG, Expanded Abstracts*, pages 2531–2535.
- Duveneck, E. (2004). Velocity model estimation with data-derived wavefront attributes. *Geophysics*, 69:265–274.
- Fomel, S. and Kazinnik, R. (2013). Non-hyperbolic common reflection surface. *Geophysical Prospecting*, 61:21–27.
- Gelchinsky, B., Berkovitch, A., and Keydar, S. (1999). Multifocusing homeomorphic imaging: Part 1. Basic concepts and formulas. *Journal of Applied Geophysics*, 42:229–242.
- Gjøystdal, H., Reinhardsen, J. E., and Ursin, B. (1984). Traveltimes and wavefront curvature calculations in three-dimensional inhomogeneous layered media with curved interfaces. *Geophysics*, 49:1466–1494.

- Höcht, G. (2002). *Traveltime approximations for 2D and 3D media and kinematic wavefield attributes*. PhD thesis, University of Karlsruhe.
- Hubral, P. and Krey, T. (1980). *Interval Velocities from Seismic Reflection Time Measurements*. SEG Monograph.
- Mayne, W. H. (1962). Common reflection point horizontal data stacking techniques. *Geophysics*, 27:927–938.
- Müller, N. A. (2007). *The 3D Common-Reflection-Surface stack – Theory and application*. PhD thesis, University of Karlsruhe.
- Müller, T. (1999). *The Common Reflection Surface stack method – seismic imaging without explicit knowledge of the velocity model*. PhD thesis, University of Karlsruhe.
- Schleicher, J., Tygel, M., Ursin, B., and Bleistein, N. (2001). The Kirchhoff-Helmholtz integral for anisotropic elastic media. *Wave Motion*, 34:353–364.
- Schwarz, B., Vanelle, C., Gajewski, D., and Kashtan, B. (2014). Curvatures and inhomogeneities: an improved common reflection surface approach. *Geophysics*, 79:S231–S240.
- Shah, P. M. (1973). Use of wavefront curvature to relate seismic data with subsurface parameters. *Geophysics*, 38:812–825.
- Spinner, M. (2007). *CRS-based minimum-aperture Kirchhoff migration in the time domain*. PhD thesis, University of Karlsruhe.
- Taner, M. T. and Koehler, F. (1969). Velocity spectra – digital computer derivation and application of velocity functions. *Geophysics*, 34:859–881.
- Tsvankin, I. (2001). *Seismic Signatures and Analysis of Reflection Data in Anisotropic Media*. Pergamon.
- Tsvankin, I. and Thomsen, L. (1994). Nonhyperbolic reflection moveout in anisotropic media. *Geophysics*, 59:1290–1304.
- Tygel, M., Müller, T., Hubral, P., and Schleicher, J. (1997). Eigenwave-based multiparameter traveltime expansions. *67th Annual International Meeting, SEG, Expanded Abstracts*, pages 1770–1773.
- Ursin, B. (1982). Quadratic wavefront and traveltime approximations in inhomogeneous layered media with curved interfaces. *Geophysics*, 47:1012–1021.
- Vanelle, C., Bobsin, M., Schemmert, P., Kashtan, B., Schwarz, B., and Gajewski, D. (2012). i-CRS: a new multiparameter stacking operator for an/isotropic media. *82nd Annual International Meeting, SEG, Expanded Abstracts*, pages 1–5.
- Vanelle, C. and Gajewski, D. (2002). Second-order interpolation of traveltimes. *Geophysical Prospecting*, 50:73–83.
- Vanelle, C., Kashtan, B., Dell, S., and Gajewski, D. (2010). A new stacking operator for curved subsurface structures. *80th Annual International Meeting, SEG, Expanded Abstracts*, pages 3609–3613.
- Xu, S. and Stovas, A. (2015). Curvature and anisotropy estimation through the CRS approximation. *Journal of Geophysics and Engineering*, 12:934–945.
- Zhang, Y., Bergler, S., and Hubral, P. (2001). Common-reflection-surface (CRS) stack for common offset. *Geophysical Prospecting*, 49:709–718.